 ICCES, vol.14, no.4, pp.103-111

Analysis of micro/mesoscale sheet stamping processes based on crystalline plasticity model

K.C. Liao[1], **C.L. Chen**[1]

Summary

A Taylor-type crystalline plasticity model, implemented into the commercial finite element analysis software, is coded as a subroutine to investigate the behavior of a stainless steel sheet with a body centered cubic (BCC) structure in the current study. Thickness variations of the sheet are examined under the micro-groove formation procedures. Effects of the spatial distribution of crystallographic orientations on the thickness distribution over the sheet are also demonstrated. Numerical results, based on the sheet with textured orientations, are in good agreement with the associated experimental measurements reported in the literature.

Keywords: crystalline plasticity, sheet metal stamping, finite element analysis.

Introduction

Developments of micro/mesoscale forming have acquired much attention due to the increasing demand of micrometallic parts in these years. A so-called size effect usually plays an important role on the metal response when characteristic dimensions, primarily referred to the grain size and the specimen/feature size, become significant under several loading conditions [Geiger, Kleiner, Eckstein, Tiesier, and Engel (2001); Kals and Eckstein (2000); Yao, Zajac, and Hutchinson (1999)].

Becker (1991) adopted a two-dimensional finite element model to examine metal material responses under the plane strain compression processes. Texture development within a grain was reported to depend not only on the misorientation of the neighboring grains, but also on the constraints provided by grains sited a few grains away. Kalidindi, Bronkhorst, and Anand (1992) demonstrated good predictive capabilities of a Taylor-type crystalline model with a fully implicit time-integration scheme. The stress-strain behavior and the texture evolution of OFHC copper based on the simulations agreed well with those based on the corresponding measurements under the simple shear and the plane strain forging processes. Harewood and McHugh (2006) utilized a finite element analysis to monitor effects of the rate-sensitivity embedded in the crystalline plasticity formulations on the accuracy of calculation results. They indicated that high mesh density might be required to capture characteristics of relatively rate-independent metals under the forming procedures. Zhao, Kuchnicki, Radovitzky, and Cuitino (2007) evaluated

[1]NTU, Taipei, Taiwan.

texture evolutions of face centered cubic metals by using three different crystalline plasticity models. The proposed direct numerical simulation approach with high mesh resolution was assessed to be able to give more accurate descriptions of the deformations and lattice rotations inside the grains. Recently Li and Zabaras (2009) implemented the rate-independent constitutive relations into a finite element model to demonstrate effects of the grain size on the uniaxial stress-strain of the metal. That smaller grain size inducing relatively stiffer stress-strain response was consistent with experimental observations.

In the past, crystalline-based models have been utilized to investigate variations of the microstructure and mechanical properties of metals under various forming procedures in the past. Beaudoin, Dawson, Mathur, Kocks, and Korzekwa (1994) applied the crystalline plasticity model to the hydroforming processes of aluminum sheets, and stated that the predicted location and height of the ears are in good agreement with the associated experiments. Nakamachi, Hiraiwa, Morimoto, and Harimoto (2000) proposed an overall hardening crystalline model with a dynamic-explicit integration scheme to demonstrate inertia effects on the deformation and the region of strain localization. Nakamachi, Xie, and Harimoto (2000) concluded that metallic textures affect the strain localization and earing under the deep drawing operations. Chen, Lee, and To (2007) also presented the influence of the initial texture of the sheet on the plastic anisotropy and formability by using the crystalline plasticity finite element approach.

Peng, Hu, Lai, Mei, and Ni (2009) examined thin sheets with different grain sizes under the micro channel fabrication processes by using the phenomenological yield criterion. They found that higher formability could be achieved for the sheet with a smaller grain size. Peng, Lai, Lee, Song, and Ni (2009) further established a uniform size dependent constitutive model to account for the behavior of the material with a relatively wide range of the size scale factor in terms of the grain size, sheet thickness, and sheet width. Peng, Lai, Lee, Song, and Ni (2009) however did not introduce severe anisotropy usually observed in sheet metals into the analysis.

A Taylor-type crystalline plasticity model is adopted here to investigate the responses of a stainless steel sheet with a body centered cubic (BCC) structure under the stamping procedures. Thickness variations of the sheet are explored and compared with the associated experimental measurements.

Constitutive Relations

From a microscopic viewpoint, a slip in a certain preferred directions on a certain preferred plane is the main mechanism of plastic deformation at a low homologous temperature. The primary advantage of the crystalline approach is that the constitutive behavior can be simulated under any loading path once the constitutive

parameters of the slip processes and grain orientations of a material are known.

Linear isotropic elasticity is assumed for the steel metal material, and a forth-order tensor of the elastic modulus C can be expressed in a form of Eq.1.

$$C = \begin{bmatrix} C_{11} & C_{12} & C_{12} & 0 & 0 & 0 \\ C_{12} & C_{11} & C_{12} & 0 & 0 & 0 \\ C_{12} & C_{12} & C_{11} & 0 & 0 & 0 \\ 0 & 0 & 0 & C_{44} & 0 & 0 \\ 0 & 0 & 0 & 0 & C_{44} & 0 \\ 0 & 0 & 0 & 0 & 0 & C_{44} \end{bmatrix} \tag{1}$$

Here elastic moduli C_{11}, C_{12}, and C_{44} is chosen as 265.2 *GPa*, 113.6 *GPa*, and 151 *GPa*, respectively [American Society for Metals (1976)].

For the $\{110\}\langle 111\rangle$ slip system assumed for BCC crystals, there are six different slip planes with two slip directions on each plane. Plastic deformation, due to the crystalline slip in metals is inherently strain rate sensitive. For rate sensitive materials, all slip systems are considered to be activated when the resolved shear stresses on the corresponding slip planes are not identically zero. Therefore, a lack of uniqueness, for the determination of the operative slip systems associated with an imposed deformation for rate insensitive materials is alleviated with the considerations of strain rate sensitivity [Pan and Rice (1983)]. A power-law relation is used to relate the resolved shear stress $\tau^{(\alpha)}$ to the shear strain rate $\dot{\gamma}^{(\alpha)}$ of the αth ($\alpha = 1, \square 12$) slip system by

$$\dot{\gamma}^{(\alpha)} = \dot{\gamma}_0^{(\alpha)} \left| \frac{\tau^{(\alpha)}}{g^{(\alpha)}} \right|^{1/m} sign(\tau^{(\alpha)}) \tag{2}$$

where $\dot{\gamma}_0^{(\alpha)}$ is the reference strain rate on the αth slip system and m represents the strain rate sensitivity of the crystalline slips. The slip system hardness, $g^{(\alpha)}$, is a function of the sum of the shear strains of all slip systems. For simplicity, the magnitude of $\dot{\gamma}_0^{(\alpha)}$ is assumed to be the same for all slip systems. The evolution of the slip system hardness is given by

$$\dot{g}^{(\alpha)} = \sum_{\beta} h_{\alpha\beta} \left| \dot{\gamma}^{(\beta)} \right| \tag{3}$$

where $h_{\alpha\beta}$, the components of the hardening matrix, gives the relationships between the hardening rate of the αth slip system and that of the βth slip system. A simple hardening matrix adopted here can be expressed as

$$h_{\alpha\beta} = q_{\alpha\beta} h^{(\beta)} \tag{4}$$

where $q_{\alpha\beta}$, the components of the matrix Q, are related to the self hardening rate on the primary slip system and the latent hardening rate on the secondary slip system of a crystal, and $h^{(\beta)}$ is a function of $g^{(\beta)}$ as

$$h^{(\beta)} = h_0 \left[1 - \frac{g^{(\beta)}}{g_s} \right]^a \tag{5}$$

Here the hardening parameters h_0, a, and the saturated slip hardness g_s are assumed to be constant for all slip systems. Note that an initial value of the slip hardness g_0 should be estimated together with Eq.5. For BCC metals, the matrix Q can be specified as

$$Q = \begin{bmatrix}
1 & q_c & q_n & q_n & q_n & q_n & q_n & q_n & q_n & q_n & q_n & q_n \\
q_c & 1 & q_n & q_n & q_n & q_n & q_n & q_n & q_n & q_n & q_n & q_n \\
q_n & q_n & 1 & q_c & q_n & q_n & q_n & q_n & q_n & q_n & q_n & q_n \\
q_n & q_n & q_c & 1 & q_n & q_n & q_n & q_n & q_n & q_n & q_n & q_n \\
q_n & q_n & q_n & q_n & 1 & q_c & q_n & q_n & q_n & q_n & q_n & q_n \\
q_n & q_n & q_n & q_n & q_c & 1 & q_n & q_n & q_n & q_n & q_n & q_n \\
q_n & q_n & q_n & q_n & q_n & q_n & 1 & q_c & q_n & q_n & q_n & q_n \\
q_n & q_n & q_n & q_n & q_n & q_n & q_c & 1 & q_n & q_n & q_n & q_n \\
q_n & q_n & q_n & q_n & q_n & q_n & q_n & q_n & 1 & q_c & q_n & q_n \\
q_n & q_n & q_n & q_n & q_n & q_n & q_n & q_n & q_c & 1 & q_n & q_n \\
q_n & q_n & q_n & q_n & q_n & q_n & q_n & q_n & q_n & q_n & 1 & q_c \\
q_n & q_n & q_n & q_n & q_n & q_n & q_n & q_n & q_n & q_n & q_c & 1
\end{bmatrix} \tag{6}$$

where q_c and q_n are assumed to be constant throughout the deformation history. They represent the ratios of the latent hardening rate of the coplanar and noncoplanar slip systems, respectively. All slip system hardening parameters above can be evaluated by the fitting of the stress-strain curve of a uniaxial tensile test.

A finite element analysis is carried out with a user-defined subroutine UMAT in ABAQUS [Hibbitt, Karlsson, and Sorensen (2008)] to illustrate deformations of the stainless steel. Selections of slip system hardening parameters incorporated in the simulations are listed in Tab. 1. Texture of a thin sheet preprocessed under the plane strain compression conditions can be obtained via a numerical analysis. Simulated {110} pole figures of the sheet with the compressive thickness strain of 0.85 shown in Fig. 1 demonstrate that (110) planes become aligned at an angle off the normal mostly in the plane defined by the surface normal and transverse direction. Uniaxial stress- strain relationship in the rolling direction based on the crystalline

plasticity finite element analysis with textured crystallographic orientations is in fair agreement with that based on experimental measurements of SUS304 sheet [Peng, Hu, Lai, Mei, and Ni (2009)], especially in the region of relatively large strain, as shown in Fig. 2. Appropriateness of the choice of these hardening parameters is therefore validated.

Table 1: Selections of slip system hardening parameters

$\dot{\gamma}_0^{(\alpha)}$	m	h_0(MPa)	a	g_s(MPa)	g_0(MPa)	q_c	q_n
0.001	0.012	500	3.2	440	60	1.2	1.4

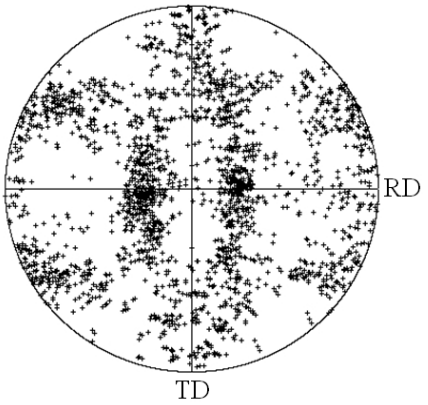

Figure 1: Simulated 110 pole figures.

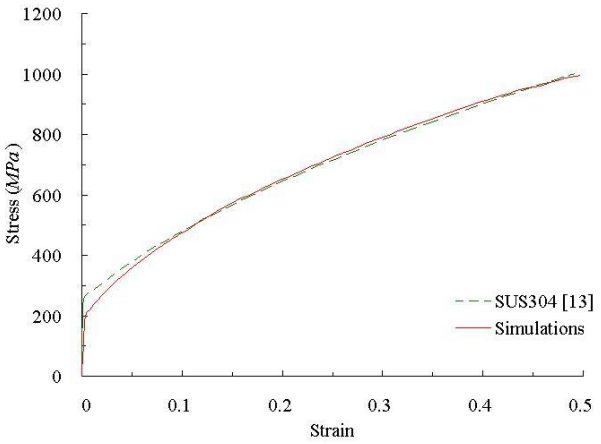

Figure 2: Uniaxial stress-strain relationships based on the finite element analysis with textured crystallographic orientations and experimental measurements of SUS304 sheet.

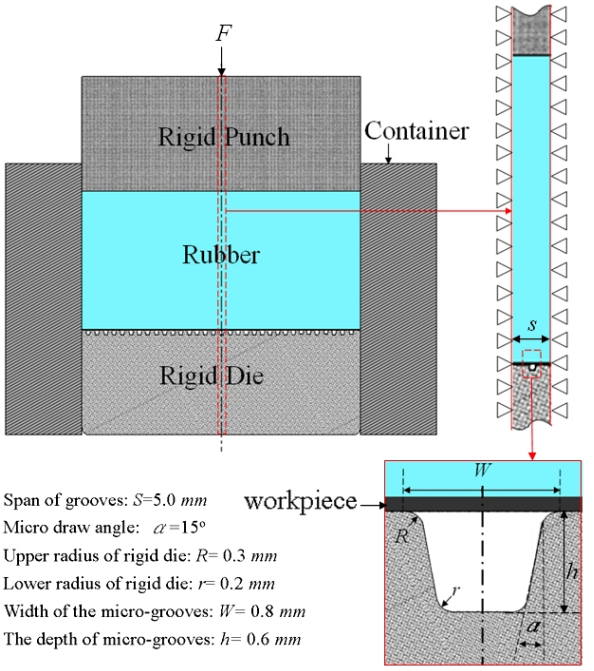

Figure 3: A schematic drawing for the micro-groove stamping.

Numerical Results

A parallel computational scheme is utilized due to the intensive calculation resource commonly required for a crystalline plasticity model. A schematic drawing with detailed dimensions for the micro-groove fabrication illustrated in Peng, Hu, Lai, Mei, and Ni (2009) is displayed in Fig. 3. A unit feature used for the finite element analysis is also shown in the figure. Since the span of the groove is much smaller than the width of the workpiece, plane strain deformation can thus be reasonably assumed. The Mooney-Rivlin model with two parameters is used to describe deformations of a hyper-elastic rubber material, while both punch and die are regarded as rigid bodies. Respectively 80 and 5 second-order plane strain quadrilateral elements along the span of the groove and the sheet thickness direction are adopted for the workpiece with a thickness of 0.1 *mm*. Initial crystallographic orientation in each element of the workpiece is extracted from the same meshed model under the plane strain compression conditions, with a compressive thickness strain of 0.85. Coulomb's friction coefficient of 0.2 is employed for the interfaces between the workpiece and soft rubber, and the workpiece and the rigid die as well. Constant punch force is then imposed to compress against the workpiece through the soft rubber. Fig. 4 shows evolutions of the von Mises equivalent stress distribution on the workpiece over the span of the groove at various deformation stages. Inhomoge-

neous stress distribution is evident as observed around the location in contact with a rounded corner of the die. Sheet thickness variations based on the simulations and the experimental measurements are demonstrated in Fig. 5 as the punch force reaches the prescribed value. Numerical results, with initially randomly distributed crystallographic orientations representing the isotropic sheet, are also included in the figure for comparisons. The distance from the original point designated in the abscissa to the centerline of the groove is 1.3 *mm*. All simulations and measurements show that the thinnest location of the workpiece occurs approximately in the region with highest equivalent stress shown in Fig. 4. Minimum thickness assessed using the model with the textured orientations agrees well with the measured value obtained from [Peng, Hu, Lai, Mei, and Ni (2009)] as shown in Fig. 5, while the model with the randomly distributed orientation dramatically underestimates the thickness in this region. Nevertheless the thickness at the grooved edge, based on the simulations is thinner than that based on the experiments.

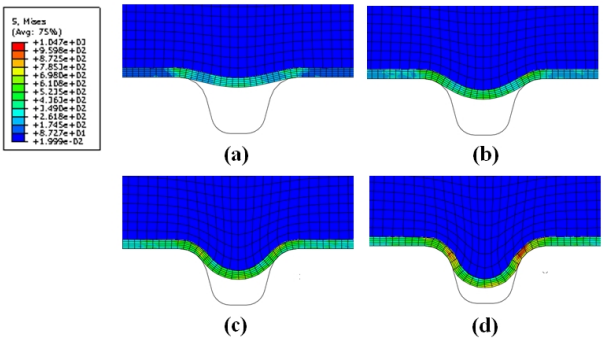

Figure 4: Evolutions of the von Mises equivalent stress distribution on the workpiece at (a) 25%, (b) 50%, (c) 75%, and (d) 100% of total deformation.

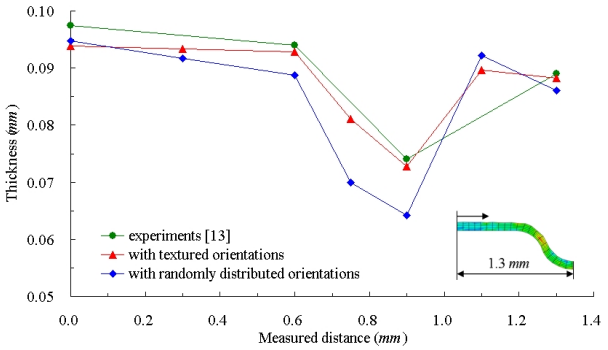

Figure 5: Final sheet thickness variations based on the simulations and the experimental measurements.

Conclusions

A crystalline plasticity model implemented into the finite element analysis could rationally assess thickness variations of stainless steel sheets under the micro-groove fabrication operations. The analysis model with the textured crystallographic orientations gives fair assessments of the sheet thickness deviation in comparison with the corresponding experimental measurements. Initial spatial distribution of crystallographic orientations exhibited in the sheet could strongly influence the thickness distribution. Effects of the implementation of various grain sizes and different orientation assignment approaches for the simulations on the material response might be expected in the future.

Acknowledgement

The authors are grateful for financial support from the National Science Council, Taiwan under contract number NSC-98-2221-E-002-020-.

References

1. **American Society for Metals** (1976): *Source book on stainless steels*. Metals Park: Ohio, pp. 14.
2. **Beaudoin, A. J.; Dawson, P. R.; Mathur, K. K.; Kocks, U. F.; Korzekwa, D. A.** (1994): Application of polycrystal plasticity to sheet forming. *Comput. Methods Appl. Mech. Eng.*, vol 117, pp. 49-70.
3. **Becker, R.** (1991): Analysis of texture evolution in channel die compression - I. Effect of grain interaction. *Acta Metal. Mater.*, vol. 39, pp.1211-1230.
4. **Chen, Y. P.; Lee, W. B.; To, S.** (2007): Influence of initial texture on formability of aluminum sheet metal by crystal plasticity FE simulation. *J. Mater. Process. Technol.*, vol. 192–193, pp.397-403.
5. **Geiger, M.; Kleiner, M.; Eckstein, R.; Tiesier, N.; Engel, U.** (2001): *Microforming*. Ann. CIRP, vol. 2, pp. 445.
6. **Harewood, F. J.; MaHugh, P. E.** (2006): Investigation of finite element mesh independence in rate dependent materials. *Comput. Mater. Sci.*, vol. 37, pp.442-453.
7. **Hibbitt, H. D.; Karlsson, B. I.; Sorensen, E. P.** (2008): *ABAQUS User Manual*. Version 6.8, USA.
8. **Kalidindi, S. R.; Bronkhorst, C. A.; Anand, L.** (1992): Crystallographic texture evolution in bulk deformation processing of fcc matel. *J. Mech. Phys. Solids.*, vol. 40, pp. 537-569.

9. **Kals, T. A.; Eckstein, R.** (2000): Miniaturization in sheet metal working. *J. Mater. Process. Technol.*, vol. 103, pp. 95–101.

10. **Li, W.; Zabaras, N.** (2009): A virtual environment for the interrogation of 3D polycrystalline microstructures including grain size effects. *Comput. Mater. Sci.*, vol. 44, pp. 1163-1177.

11. **Nakamachi, E.; Hiraiwa, K.; Morimoto, H.; Harimoto, M.** (2000): Elastic/crystalline viscoplastic finite element analyses of single and poly-crystal sheet deformations and their experimental verification. *Int. J. Plast.*, vol. 16, pp. 1419-1441.

12. **Nakamachi, E.; Xie, C. L.; Harimoto, M.** (2000): Drawability assessment of bcc steel sheet by using elastic/crystalline viscoplastic finite element analyses. *Int. J. Mech. Sci.*, vol. 43, pp.631-652.

13. **Pan, J.; Rice, J. R.** (1983): Rate sensitivity of plastic flow and implications for yield-surface vertices. *Int. J. Solids Struct.*, vol. 19, pp. 973-987.

14. **Peng, L.; Hu, P.; Lai, X.; Mei, D.; Ni, J.** (2009): Investigation of micro/ meso sheet soft punch stamping process- simulation and experiments. *Materials and design*, vol.30, pp.783-790.

15. **Peng, L.; Lai, X.; Lee, H. J.; Song, J. H.; Ni, J.** (2009): Analysis of micro/ mesoscale sheet forming process with uniform size dependent material constitutive model. *Mater. Sci. Eng.*

16. ***A***, vol. 526, pp. 93-99.

17. **Yao, X.; Zajac, S.; Hutchinson, B.** (1999): Estimation of compression flow stress from post-deformation hardness in Al-Mg alloys. *Script. Mater.*, vol. 41, no. 3, pp. 95-101.

18. **Zhao, Z.; Kuchnicki, S.; Radovitzky, R.; Cuitino, A.** (2007): Influence of in-grain mesh resolution on the prediction of deformation textures in fcc polycrystals by crystal plasticity FEM. *Acta Mater.*, vol.55, pp.2361-2373.